


Stable electromagnetic interactions with effective media of active multilayersConstantinos Valagiannopoulos **Department of Physics, School of Sciences and Humanities, Nazarbayev University, Nur-Sultan 010000, Kazakhstan*

(Received 22 September 2021; revised 18 December 2021; accepted 20 December 2021; published 18 January 2022)

Gain is a blessing and a curse for photonic designs; indeed, gain-based devices may become unprecedentedly efficient but, on the other hand, the local electromagnetic fields can increase exponentially with time and lead the systems to instability. Such stability considerations are presented for a homogenized configuration incorporating tilted active multilayers by determining the poles of its transfer functions across the complex frequency plane and analytically deriving the respective constraints. The reported stable regimes will be crucial in tuning the examined module when incorporated in photonic setups for serving multiple purposes from filtering and imaging to cloaking and lasing.

DOI: [10.1103/PhysRevB.105.045304](https://doi.org/10.1103/PhysRevB.105.045304)**I. INTRODUCTION**

Designs incorporating gain media can easily surpass performance bars posed by passive setups and lead to unparalleled levels of tunability and control, since they are able to reformulate the energy equilibrium without being quantitatively restricted by the primary excitation power [1,2]. Active configurations have been fabricated to achieve perfect electromagnetic cloaking [3], ultraefficient polarization engineering [4], and flawless reflection phase calibration [5], being indispensable for a large range of integrated optical systems. In addition, lasing constitutes a significant category of photonic operations that employ materials with gain and has been experimentally accomplished with coupled plasmonic nanocavity arrays [6], microrings of periodically placed bilayers [7], or hybrid core-shell nanoparticles [8]. Parity-time (PT) symmetry is also a design strategy allowing a controlled interplay between gain and loss that develops reconfigurable light transport [9], unidirectional matching [10], and spatiotemporal solitons [11]. All these fascinating findings have recently ignited substantial funding initiatives encouraging research on active topological metastructures [12], advanced functional media [13], and responsive texture with gain [14], that are expected to deliver even more efficient electromagnetic setups in the near future.

However, the use of active materials may jeopardize the stability of the hosting devices; namely, these substances can pump unlimited amounts of energy and produce fields that increase exponentially with time, having an apparently disastrous outcome [15]. That is why a careful stability analysis is mandatory every time one employs gain in a photonic design that interacts with light; otherwise, the reported resonant regimes may not be attainable [16]. In particular, parametric combinations that respect the stability constraints are necessary in order to create frequency combs induced by phase turbulence [17], sustain injection locking in semiconductor

lasers [18], and develop nonlinear resonances in active couplers [19,20] or photonic oscillators [21]. Importantly, thorough stability considerations are provided for effects like active scattering-cancellation cloaking [22], PT-symmetric invisibility [23], spectral singularities [24], and superscattering in non-Hermitian cylindrical structures [25]. Similar stability checks are core to studies investigating planar [26] and cylindrical [27] metasurfaces for volumetric imaging as well as non-Foster circuits with active components [28,29] and negative capacitors [30].

One of the simplest and analytically solvable geometries when modeling electromagnetic interactions contains periodic stacks of multiple layers; some of the most important photonic properties, like negative refractive index [31] or hyperbolic dispersion [32,33], have been first experimentally demonstrated in analogous layered structures. Broadband absorption of the incoming illumination is also attained with stacked plasmonic films in the visible [34], terahertz [35], and microwave [36] frequencies, while the coupling between fully anisotropic graphene multilayers [37] have been successfully used in the design of tunable infrared plasmonic devices [38]. Furthermore, homogenization of alternating films with different texture give effective permittivity tensors [39] that correspond to zero-index optical metamaterials [40]. Similar setups exploit the constructive and destructive interference of waves to model maximally controllable modules [41], efficient photovoltaic components [42], and highly selective transmitters [43].

In this work, we investigate the stability of such a ubiquitous component, finite in thickness, when one of the periodically stacked media is active; in particular, a passive slab hosts multiple tilted thin films with gain. The optical axis of the corresponding effective anisotropic medium is rotated and the structure is fed by obliquely incident waves of arbitrary polarization. It is important to note that the actual periodic configuration is replaced by a homogenized uniaxial material; therefore, all the subsequent results are valid only if the textural discontinuity between multilayers and passive background does not severely affect the developed scattering

*konstantinos.valagiannopoulos@nu.edu.kz

effects. Analytical derivation for the poles of the transfer functions at the complex frequency plane is provided and the corresponding stability constraints are formulated. The transmissivity across various parametric maps is presented under the conditions for stable operation and the parametric selections leading to significant pumping of energy are identified. In particular, by choosing properly the gain levels and the incoming illumination direction, one can safely produce fields several orders of magnitude stronger than the input ones, while a proper tilt of the active layers can substantially enhance the systemic stability. The reported findings shed light upon the stable modes of these versatile photonic modules and can be critical when designing integrated setups that embody them.

II. STABILITY CONSIDERATIONS

A. Problem statement

The structure under consideration is depicted in Fig. 1(a), where the used Cartesian coordinate system (x, y, z) is also defined. A slab of thickness h is filled with a medium of relative complex permittivity ε_1 and loaded with parallel thin strips of another medium with relative complex permittivity ε_2 . These thin films are tilted by angle φ with respect to the horizontal x axis and the filling factor of ε_2 into ε_1 host is denoted by $0 < r < 1$. The configuration exists into free space and can be excited by plane waves with frequency ω of both polarizations: TM (sole electric field $\mathbf{E} \parallel \hat{\mathbf{z}}$) and TE (sole magnetic field $\mathbf{H} \parallel \hat{\mathbf{z}}$) traveling along a direction forming an angle θ with the horizontal x axis. Note that the period of the lattice into the slab is d and a secondary Cartesian coordinate system (X, Y, z) is indicated, with its X axis parallel to the boundaries of the internal layers.

A harmonic dependence of time with the form $\exp(-i\omega t)$ is assumed, which means that a negative imaginary part $\text{Im}[\varepsilon] < 0$ of complex permittivity ε corresponds to gain and a positive one $\text{Im}[\varepsilon] > 0$ indicates losses. As always, a $\text{Re}[\varepsilon] > 1$ corresponds to a dielectric behavior and a $\text{Re}[\varepsilon] < 1$ is related to plasmonic response. One or both of the employed media ($\varepsilon_1, \varepsilon_2$) can be active in a direct or an effective way via time modulation [44] and, thus, instability may occur. Therefore, our mission will be to derive the conditions for stable operation and, once they are respected, investigate the response of the device.

If we denote by F_z the z component of the corresponding sole field in each case ($F_z = E_z$ for TM modes and $F_z = H_z$ for TE modes), the Fourier transform of the transmissive field behind the considered slab is given by $F_z(\omega, x, y) = T(\omega)e^{+ik(x \cos \theta + y \sin \theta)}$. The symbol $T(\omega)$ is used for the complex transmission coefficient, playing the role of the transfer function, $k = \omega/c$ is the operational free-space wave number, and c is the speed of light into vacuum. In the presence of noise with spectrum $Q(\omega)$, the time-dependent transmissive field can be written as

$$f_z(t, x, y) = \int_{-\infty}^{+\infty} Q(\omega)T(\omega)e^{-i\omega t + i\frac{\omega}{c}(x \cos \theta + y \sin \theta)} d\omega. \quad (1)$$

As designated in Fig. 1(b), the integral (1) can be evaluated by deforming the Fourier integration path and following an infinite semicircle at the lower half plane of complex frequency

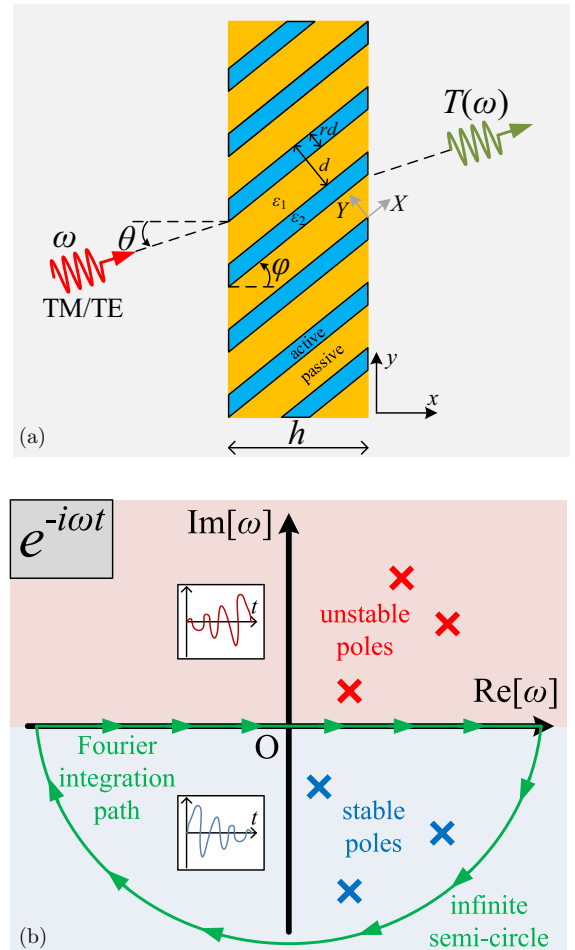


FIG. 1. (a) Physical configuration of the considered setup: a passive slab of thickness h and relative permittivity ε_1 hosts strips of active medium with relative permittivity ε_2 . The optical axis X of the slab is tilted by angle φ and the structure is illuminated by a TM/TE plane wave of frequency ω traveling across direction forming an angle θ with the horizontal axis x . The transmission coefficient is denoted by $T(\omega)$. (b) Sketch of the poles of the transfer function $T(\omega)$ positioned on the complex frequency ω plane. Due to the bypass of the Fourier integral, residues give exponentially decreasing (stable) or increasing (unstable) time variations.

ω , across which the integrand exponentially vanishes for $t > 0$ due to the factor $e^{-i\omega t}$. By taking into account that the noise spectrum $Q(\omega)$ exciting the device cannot be singular, one directly infers that the integral (1) is proportional to the residues of $T(\omega)$ at the unstable complex poles $\omega = \tilde{\omega}$ of $T(\omega)$ belonging in the upper half space. In this way, the field will explode like $f_z(t, x, y) \sim \exp(-i\tilde{\omega}t)$ in the presence of at least one unstable pole $\tilde{\omega}$ of $T(\omega)$ with $\text{Im}[\tilde{\omega}] > 0$ or asymptotically vanish if all the poles $\tilde{\omega}$ of $T(\omega)$ are stable ($\text{Im}[\tilde{\omega}] < 0$). That is why we show the representative variations with time t in the insets of Fig. 1(b) for each of the two cases.

B. Electromagnetic fields

If one assumes that the period d of the periodically located films of Fig. 1(a) is much smaller than the wavelength $\lambda \equiv 2\pi c/\omega = 2\pi/k$, the effective relative permittivities along

the axes (X, Y) are given by $\varepsilon_X = (1 - r)\varepsilon_1 + r\varepsilon_2$ and $\varepsilon_Y = \frac{\varepsilon_1\varepsilon_2}{(1-r)\varepsilon_2 + r\varepsilon_1}$, based on well-known homogenization formulas [34]. Hence the relative permittivity tensor $[\varepsilon]$ in the global Cartesian coordinate system (x, y, z) takes the form [41]

$$[\varepsilon] = \begin{bmatrix} \varepsilon_{xx} & \varepsilon_{xy} & 0 \\ \varepsilon_{xy} & \varepsilon_{yy} & 0 \\ 0 & 0 & \varepsilon_X \end{bmatrix} = \begin{bmatrix} \varepsilon_X \cos^2 \varphi + \varepsilon_Y \sin^2 \varphi & (\varepsilon_X - \varepsilon_Y) \cos \varphi \sin \varphi & 0 \\ (\varepsilon_X - \varepsilon_Y) \cos \varphi \sin \varphi & \varepsilon_Y \cos^2 \varphi + \varepsilon_X \sin^2 \varphi & 0 \\ 0 & 0 & \varepsilon_X \end{bmatrix}. \quad (2)$$

When the electric field is parallel to the z axis (TM polarization), we write $E_z = e^{+iky \sin \theta} [A e^{+ik\kappa_{\text{TM}}x} + B e^{-ik\kappa_{\text{TM}}x}]$, where

$$\kappa_{\text{TM}} = \sqrt{\varepsilon_X - \sin^2 \theta}. \quad (3)$$

Once the magnetic field is parallel to z axis (TE polarization), the Helmholtz equation gives $H_z = e^{+iky \sin \theta} e^{-ik \frac{\varepsilon_{xy}}{\varepsilon_{xx}} x \sin \theta} [A e^{+ik\kappa_{\text{TE}}x} + B e^{-ik\kappa_{\text{TE}}x}]$, where

$$\kappa_{\text{TE}} = \sqrt{(\varepsilon_{xx} - \sin^2 \theta) \left(\frac{\varepsilon_{yy}}{\varepsilon_{xx}} - \frac{\varepsilon_{xy}^2}{\varepsilon_{xx}^2} \right)}. \quad (4)$$

The quantities A, B are arbitrary complex coefficients. Note that $\text{Re}[\kappa_{\text{TM/TE}}] > 0$, since it is always taken positive by convention.

The homogenization process [45] of replacing an actual layered structure by an effective uniaxial medium with permittivity described by (2) is not always successful. Indeed, reflectivity from all-dielectric multilayers of deeply subwavelength thickness cannot be well predicted via effective-medium theory when the structure is excited obliquely via a dense semicylindrical prism made of zinc selenide [46]. Similarly, it has been shown [47] that a single subwavelength inclusion can have a dramatic effect in an one-dimensional disordered optical system under specific illumination angles while the homogenization fails when the permittivity difference is small [43]. Furthermore, nanophotonic disorders give strong field localization [48], while extremely thin optical coatings can substantially boost the absorbing efficiency of plasmonic slabs [49].

However, we advocate that the aforementioned weak points of effective-medium theory do not significantly affect the validity of the results presented in our study. First of all, the model is perfectly accurate in the case that we do not regard a layered structure but an inherently uniaxially anisotropic substance. But, even for the considered multilayers, the breakdown of the effective-medium approximation potentially occurs for discrete, singular incidence directions θ ; that feature means that our conclusions for all the other angles are correct. As indicated below, we search for constraints leading to conditional stability, namely, stable operation if the features of the incoming beam (polarization, wavelength, angle) are taken constant; therefore, the critical angles for total internal reflection, at which the effective-medium theory potentially fails, can be excluded from the regarded θ spectrum.

Moreover, in all the aforementioned works reporting failure of the effective-medium model [43,46–49], the incoming beam meets a setup with layers of infinite length $h/\cos \varphi \rightarrow +\infty \Rightarrow \varphi = 90^\circ$; here, we have a configuration of tilted optical axis which gives a full permittivity tensor. As a result, the developed waves possess more complex forms and, thus, achieving a combination of angles leading to the internal reflection regime becomes more challenging. Furthermore, in some of these papers [46,48] the breakdown of the homogenization model happens when the layout is fed by evanescent waves exiting a high-permittivity dielectric prism, which is not the case in the present study where propagating fields are exciting the device.

Despite all these arguments in favor of the suitability of the employed approximations, we tested some representative designs examined in this work by comparing the electromagnetic signal distribution when simulating the actual layered structures via commercial software COMSOL MULTIPHYSICS [50], with the one derived when implementing the effective-medium approximation. We have found, for a variety of slab thicknesses, tilt angles, and by using omnidirectional line sources containing all possible incidence angles θ , that the two sets of data are qualitatively and quantitatively similar both into vacuum and into the layered modules. The results are not shown here for brevity but any discrepancies can be attributed to the granularity of the used meshing required by the applied finite element method and not to a systematic breakdown of effective-medium theory for specific parametric sets.

C. Stability constraints

If one considers a source-free version of the problem depicted in Fig. 1(a), the fields into the two semi-infinite vacuum regions will be outgoing from the structure. After imposing continuity for the tangential electric and magnetic components along the interfaces $x = 0, h$ and eliminating the redundant complex coefficients, it is found that the considered structure may support electromagnetic waves only if the following constraints are satisfied:

$$e^{+i \frac{\omega}{\omega_0} k_0 h \kappa_{\text{TM}}} = \pm \frac{1 + \kappa_{\text{TM}} \sec \theta}{1 - \kappa_{\text{TM}} \sec \theta} \equiv \pm G_{\text{TM}}, \quad (5)$$

$$e^{+i \frac{\omega}{\omega_0} k_0 h \kappa_{\text{TE}}} = \pm \frac{u + \varepsilon_{xx} \kappa_{\text{TE}} \sec \theta}{u - \varepsilon_{xx} \kappa_{\text{TE}} \sec \theta} \equiv \pm G_{\text{TE}}, \quad (6)$$

for each type of field (TM or TE respectively), where $u = \varepsilon_{xx}\varepsilon_{yy} - \varepsilon_{xy}^2$. The quantity $\omega_0 > 0$ is a reference frequency dictated by the application for which we operate the device and $k_0 = \omega_0/c$ is the respective free-space wave number.

If one assumes that the quantities $G_{\text{TM/TE}}$ are not dependent on the oscillation frequency ω , Eqs. (5) and (6) can be rigorously solved with respect to complex ω which, as will become obvious later in the analysis, constitute the poles of the system's transfer functions $T(\omega)$. Their exact expressions are given by

$$\text{Re} \left[\frac{\omega}{\omega_0} \right] = \frac{\text{Re}[\kappa](m\pi + \arg[G]) - \text{Im}[\kappa] \ln |G|}{k_0 h |\kappa|^2}, \quad (7)$$

$$\text{Im} \left[\frac{\omega}{\omega_0} \right] = - \frac{\text{Im}[\kappa](m\pi + \arg[G]) + \text{Re}[\kappa] \ln |G|}{k_0 h |\kappa|^2}, \quad (8)$$

where $m \in \mathbb{Z}$ and $\kappa = \kappa_{\text{TM/TE}}$ and $G = G_{\text{TM/TE}}$ in proportion to the wave polarization we investigate. The poles lie along a straight line with slope $-\text{Im}[\kappa]/\text{Re}[\kappa]$, whose sign is decided by $\text{Im}[\kappa]$ since $\text{Re}[\kappa] > 0$, according to (3) and (4). To ensure stability, these poles should belong to the lower half complex plane ($\text{Im}[\omega] < 0$) by keeping a positive real part ($\text{Re}[\omega] > 0$); otherwise, the time dependence $\exp(-i\omega t)$ loses its true meaning. Therefore, we have a stable operation once

$$\text{Im}[\kappa](m\pi + \arg[G]) + \text{Re}[\kappa] \ln |G| > 0, \quad (9)$$

for every single integer $m \in \mathbb{Z}$ with $m > \frac{\text{Im}[\kappa] \ln |G| - \text{Re}[\kappa] \arg[G]}{\pi \text{Re}[\kappa]}$. By inspection of (9), it is clear that $\text{Im}[\kappa] > 0$ is a prerequisite for stability since only then the inequality is obeyed for $m \rightarrow +\infty$. If one takes into account the minimum m for which (9) should be satisfied, the sufficient conditions for stable operation read

$$\text{Im}[\kappa_{\text{TM/TE}}] > 0, \quad |G_{\text{TM/TE}}| > 1. \quad (10)$$

It is noted that, for the simplest of the two polarizations (TM), we obtain [51]

$$|G_{\text{TM}}|^2 = 1 + \frac{4 \text{Re}[\kappa_{\text{TM}}] \cos \theta}{\text{Im}^2[\kappa_{\text{TM}}] + (\text{Re}[\kappa_{\text{TM}}] - \cos \theta)^2}, \quad (11)$$

meaning that the second of the two constraints in (10) is automatically true for TM waves. Indeed, $\text{Re}[\kappa_{\text{TM}}] > 0$ as the real part of a square root and $\cos \theta > 0$ because $-90^\circ < \theta < 90^\circ$ for the definition of incidence angle θ in Fig. 1(a). An expression similar to (11) can be numerically obtained for TE waves and, therefore, we draw the conclusion that the most important inequalities from those in (10) are the first ones, regardless of the type of excitation.

Given the fact that noise exists everywhere along the frequency axis ω via the random spectrum $Q(\omega)$ of (1) and is a signal containing any sort of wave, the stability of the system is judged on the basis of imposing (10) for both the working polarizations. However, in the following, we will investigate the conditional stability of the system by assuming that characteristics of the illumination like the type (TM/TE) and the incidence angle (θ) are kept constant, in the same way that the angular momentum order has been taken fixed in a cylindrical analog [25]. Our aim is to examine the behavior of the device under the assumption that an efficient filter is employed to block any other, deterministic or stochastic, incoming signal except for that of the specific angle and polarization; similar postulations hold for all the numerical results. Thus, in the following, the conditions (10) will be considered separately for each field type and for specific incoming wave direction.

Another interesting aspect of the investigated configuration concerns its non-Hermitian characteristics due to the inclusion of active layers. In particular, the creation of stable electromagnetic signals within such structures is similar to the development of constant intensity waves in non-Hermitian systems involving loss and gain [52], where the scattering is counterbalanced by pumping extra energy [53]. Similarly, these devices can achieve independent control of amplitude and phase of the fields; such a concept is proven via a Bohmian reformulation to Maxwell's equations [54].

D. Nondispersive media conjecture

The derivations of the poles (7) and (8) and the subsequent stability constraints (10) are based on the conjecture that $G_{\text{TM/TE}}$ and $\kappa_{\text{TM/TE}}$ are independent from the operational frequency ω . However, the retardation of oscillating atoms and the physical principle of causality, stating that the output of a system cannot temporally precede the input, calls for dispersive media [27]. The most common frequency variation of a material's permittivity is given by the well-known Lorentz model:

$$\varepsilon(\omega) = 1 \mp \frac{\omega_p^2}{i\omega\Gamma + \omega^2 - \omega_0^2}. \quad (12)$$

The minus sign corresponds to passive designs and the plus sign describes active ones for $\Gamma > 0$. Note that, just by flipping the sign of losses Γ , one obtains an active but noncausal electrical response. The dispersive permittivity (12) implies that the impulse response of a medium comprises of a delta function at $t = 0$ and a damped oscillation beginning at $t = 0$. According to this scenario, each atom of the material is conceptually simulated by a spring whose resonance frequency is denoted by ω_0 and damping frequency by Γ ; the third frequency ω_p is called plasma frequency being proportional to the number of atoms into the volume of the material.

If ε_1 and ε_2 are characterized by dispersion (12), the functions $G_{\text{TM/TE}}(\omega)$ and $\kappa_{\text{TM/TE}}(\omega)$ will be dependent on complex ω . Thus the explicit deduction of the poles like in (7) and (8) will be infeasible and, accordingly, closed-form stability constraints as in (10) will not be easily derived; on the contrary, cumbersome numerical determination of the roots across the entire complex ω plane will be required every single time the setup alters. For this reason, we will hereinafter work with the rules (10) to understand the approximate stability dynamics of the system in Fig. 1(a). More specifically, we will assume that the permittivities are dispersion free ($\varepsilon_1, \varepsilon_2$ independent from ω). Alternatively, one may suppose that the central operational frequency $\omega = \omega_0$ belongs to a range across which the function $\varepsilon(\omega)$ is relatively flat, a feature that can involve Lorentz-type variation (12).

Another implication of dispersion-free assumption is that we search for unstable poles (upper complex half plane, $\text{Im}[\omega] > 0$) that have strictly positive real parts ($\text{Re}[\omega] > 0$). Even though poles appear at the upper left quarter of the complex ω plane, we will ignore them since the actual singularities with $\text{Re}[\omega] < 0$ are directly determined via the poles with $\text{Re}[\omega] > 0$. In particular, the transfer function $T(\omega)$ is characterized by the property $T(-\omega^*) = T^*(\omega)$ because the electric field response in time should be real [55,56]; as a result, its poles are placed symmetrically with respect to the imaginary $\text{Re}[\omega] = 0$ axis. Hence a transfer function that does not become singular at the $\{\text{Im}[\omega] > 0, \text{Re}[\omega] > 0\}$ quadrant will describe a stable system.

III. STABLE OPERATION

A. Transmissivity derivation

When the structure is illuminated by a plane wave with magnetic or electric field always parallel to z axis given by

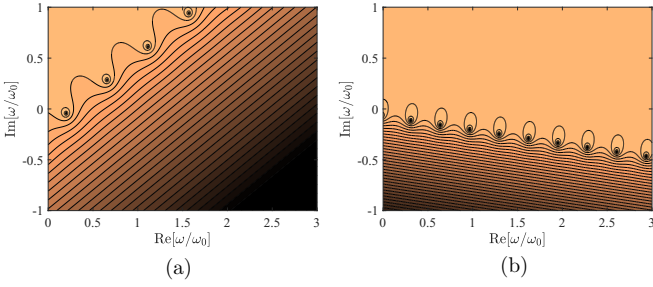


FIG. 2. Transfer function magnitude $|T(\omega)|$ represented across the complex frequency ω plane for (a) TM waves (unstable) and (b) TE waves (stable). Plot parameters: $\varepsilon_1 = 1 + 2i$, $\varepsilon_2 = 1 - 8i$, $r = 0.5$, $\varphi = 30^\circ$, $\theta = 0^\circ$, and $h = \lambda/2$.

$F_z = e^{+iky \sin \theta + ikx \cos \theta}$, the boundary conditions at $x = 0, h$ determine the following transmission coefficients:

$$T_{\text{TM}} = \frac{4\kappa_{\text{TM}} \cos \theta}{(\kappa_{\text{TM}} - \cos \theta)^2} \frac{e^{+ikh(\kappa_{\text{TM}} - \cos \theta)}}{G_{\text{TM}}^2 - e^{+2ikh\kappa_{\text{TM}}}}, \quad (13)$$

$$T_{\text{TE}} = \frac{4\kappa_{\text{TE}} \varepsilon_{xx} u \cos \theta}{(\varepsilon_{xx} \kappa_{\text{TE}} - u \cos \theta)^2} \frac{e^{+ikh(\kappa_{\text{TE}} - \cos \theta - \frac{\varepsilon_{xy}}{\varepsilon_{xx}} \sin \theta)}}{G_{\text{TE}}^2 - e^{+2ikh\kappa_{\text{TE}}}}, \quad (14)$$

for each of the two considered polarizations (TM/TE). Note that the poles of $T_{\text{TM/TE}}$ are the roots of the transcendental Eqs. (5) and (6), respectively, whose explicit forms are expressed by (7) and (8).

In Fig. 2, we represent the transfer functions for both types of waves (TM/TE) across the complex frequency ω plane and we realize that an active design can be stable for the one polarization but unstable for the other. In particular, Fig. 2(a) demonstrates the variation of $|T_{\text{TM}}(\omega)|$ and the poles lie along a straight line, as dictated by (7) and (8). The first pole is stable but all the others possess larger imaginary parts and belong to the upper half of the complex ω plane. On the contrary, for TE waves [Fig. 2(b)], the locus of the poles is a downward sloping curve due to the different sign of $\text{Im}[\kappa_{\text{TE}}] > 0$ and its entirety is included into the stable half space.

B. Permittivities planes

The imaginary parts of the permittivities ($\varepsilon_1, \varepsilon_2$) are crucial quantities determining the stability of the photonic setups; therefore, the variation of the device output with respect to them is meaningful and should be studied. In Fig. 3, we show on the map $(\text{Im}[\varepsilon_1], \text{Im}[\varepsilon_2])$ the transmissivity expressed in dB; the blank regions correspond to instability. In Fig. 3(a), where TM waves are considered, half of the inspected parametric region sends the system to unbounded oscillations since we have assumed that both the media occupy the same volume in the layered configuration ($r = 0.5$). Note that the response of the setup gets stronger when the imaginary parts are selected smaller and, once the line $\text{Im}[\varepsilon_1] + \text{Im}[\varepsilon_2] = 0$ is crossed, the structure becomes unstable; thus, in this case, the instability occurs when transmission increases. With blue marker \times , we denote the design examined in Fig. 2, which is unstable for TM waves.

In Fig. 3(b), we assume TE excitation and understand that the response is not exclusively dependent on the quantity

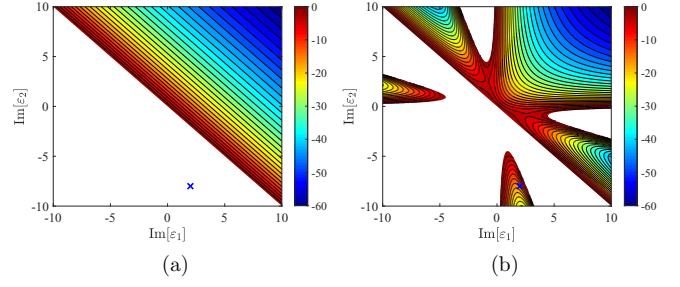


FIG. 3. Transmissivity $|T|^2$ in dB with respect to the imaginary parts of relative permittivities of the two media ($\text{Im}[\varepsilon_1], \text{Im}[\varepsilon_2]$). (a) TM waves; (b) TE waves. Plot parameters: $\text{Re}[\varepsilon_1] = \text{Re}[\varepsilon_2] = 1$, $r = 0.5$, $\varphi = 30^\circ$, $\theta = 0^\circ$, and $h = \lambda/2$. The blue markers \times denote the design with transfer functions examined by Fig. 2. Blank regions indicate instability.

$(\text{Im}[\varepsilon_1] + \text{Im}[\varepsilon_2])$. More specifically, the instability domain is not anymore coherent and thus two blank regions appear in the upper right part of the permittivity map while two stable ones emerge at the lower left half. That is why the [same as that of Fig. 3(a)] design marked with blue pointer \times is now stable, as indicated by the poles of its TE transfer function in Fig. 2(b). However, it should be stressed that, even with this alternative polarization, the response is always unstable when both materials are active ($\text{Im}[\varepsilon_1], \text{Im}[\varepsilon_2] < 0$) and, of course, the system is stable when the two media are passive ($\text{Im}[\varepsilon_1], \text{Im}[\varepsilon_2] > 0$). It is also noteworthy that across all the instability boundaries of Fig. 3(b) the system gives substantial transmissivity (close to its maximal unitary value), as also happens in Fig. 3(a).

In Fig. 4, we regard the map of real parts of permittivities and identify the different influence they have on the stability of the considered slab for different incoming wave polarizations. In Fig. 4(a), where TM fields are examined, we obtain an always-stable response with variation complementary to that of Fig. 3(a), namely, $|T_{\text{TM}}|^2$ increases for increasing $(\text{Re}[\varepsilon_1] + \text{Re}[\varepsilon_2])$. Importantly, the real parts of dielectric constants ($\varepsilon_1, \varepsilon_2$) do not seem to affect substantially the TM stability of the layout, at least in this specific design. In Fig. 4(b), we assume TE waves and a large instability region around the $\text{Re}[\varepsilon_2] = 0$ line is formulated, which is almost symmetric with respect to the $\text{Re}[\varepsilon_1] = 0$ axis. In particular, the more

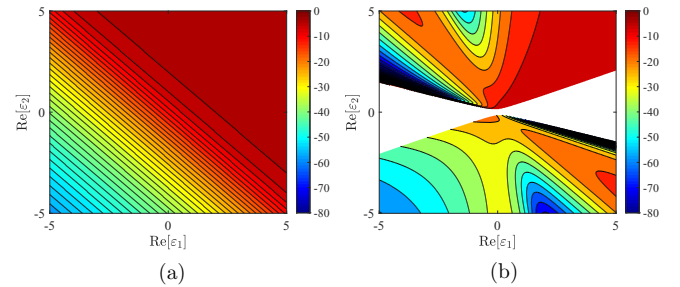


FIG. 4. Transmissivity $|T(\omega)|^2$ in dB with respect to the real parts of relative permittivities of the two media ($\text{Re}[\varepsilon_1], \text{Re}[\varepsilon_2]$). (a) TM waves; (b) TE waves. Plot parameters: $\text{Im}[\varepsilon_1] = 0.8$, $\text{Im}[\varepsilon_2] = -0.2$, $r = 0.5$, $\varphi = 30^\circ$, $\theta = 0^\circ$, and $h = \lambda/2$. Blank regions indicate instability.

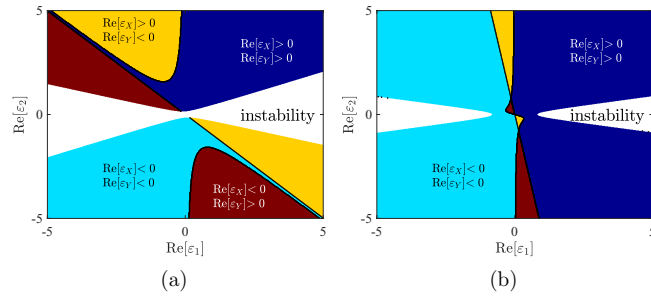


FIG. 5. Signs of the real parts of the effective permittivities (ε_X , ε_Y) on the map of the real parts of the permittivities of the original media (ε_1 , ε_2). (a) The identical case examined in Fig. 4(b) ($r = 0.5$). (b) Same case examined in Fig. 4(b) but with $r = 0.15$.

substantial $|\text{Re}[\varepsilon_1]|$ is, the more challengingly one achieves stability via selecting $\text{Re}[\varepsilon_2]$ and vice versa. Interestingly, the transmissivity of the slab just before entering the unstable region is not necessarily equal to maximum; in some cases, the response can even vanish.

This finding may sound peculiar since instability is subconsciously related with huge field magnitudes. However, what we represent in Figs. 3 and 4 is the magnitude of the phasors of the transmissive fields $|F_z|$, under the assumption that the system converges to finite responses. Indeed, the decision regarding the instability or not of a system is not made by the magnitude of the signal f_z at a specific time (say, $t = 0$) but by the evolution of the signal as the time t goes by. In other words, in the presence of white noise $Q(\omega)$, a configuration represented by a nonblank point (ε_1 , ε_2) on the maps of Figs 3 and 4 will produce transmissive waves of magnitude $|T(\omega)|$ that vanish with time. On the other hand, if the point (ε_1 , ε_2) is blank, the transmission will explode with time like $\exp(-i\tilde{\omega}t)$, as imposed by the unstable pole $\omega = \tilde{\omega}$, but at $t = 0$ will be finite too and proportional to $T(\tilde{\omega})$. Nonetheless, we avoid showing these finite values since the system is unstable. It is, therefore, directly inferred that one should not confuse the amplification scenario of $|T(\text{Re}[\tilde{\omega}])|^2 > 1$ with the unstable regime concerning an exponentially increasing quantity $T \exp(-i\tilde{\omega}t)$ with time t .

It would be also interesting to investigate the nature of the effective media expressed via the permittivities (ε_1 , ε_2) and thus we identify four distinct regions on the parametric plane ($\text{Re}[\varepsilon_1]$, $\text{Re}[\varepsilon_2]$), as in Fig. 4, in proportion to the signs of the real parts of the homogenized permittivities (ε_X , ε_Y). Dark blue domains describe a dielectric uniaxial material, while light blue areas indicate a plasmonic substance. Similarly, yellow and brown colors are used for hyperbolic media, while blank regions correspond again to permittivity combinations leading to instability for the given amounts of gain and loss. In Fig. 5(a), we consider the same system examined in Fig. 4(b) under TE excitation since only then the effective medium is anisotropic; indeed, one directly observes that numerous combinations of (ε_1 , ε_2) examined in Fig. 4(b) give equivalent materials with hyperbolic dispersion relation. By juxtaposing Figs. 4(b) and 5(a), it is clear that when the hyperbolic homogenized material has $\text{Re}[\varepsilon_X] < 0$ the transmissivity is, on average, much weaker than in the hyperbolic scenario with $\text{Re}[\varepsilon_X] > 0$. Importantly, the isocontour levels of $|T_{\text{TE}}|^2$

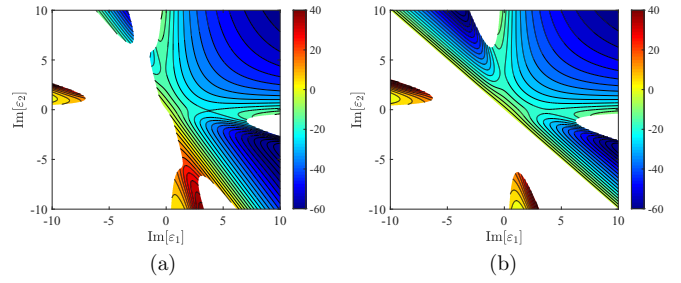


FIG. 6. Transmissivity $|T|^2$ in dB with respect to the imaginary parts of relative permittivities of the two media ($\text{Im}[\varepsilon_1]$, $\text{Im}[\varepsilon_2]$). (a) $r = 0.4$; (b) $r = 0.5$. Plot parameters: $\text{Re}[\varepsilon_1] = \text{Re}[\varepsilon_2] = 1$, $r = 0.5$, $\varphi = 30^\circ$, $\theta = -45^\circ$, and $h = \lambda/2$. Only TE type of excitation is considered. Blank regions indicate instability.

of Fig. 4(b) have conformal shapes with the boundaries of different regions of Fig. 5(a). In Fig. 5(b), we repeat the calculations of a structure identical to that of Fig. 5(a) but for active layers with smaller filling factor ($r = 0.15$). It is remarked that the domains of permittivities ($\text{Re}[\varepsilon_1]$, $\text{Re}[\varepsilon_2]$) giving hyperbolic dispersion get substantially shrunk; the same happens with the unstable regions since the volume of the gain medium decreases too. Finally, the symmetry of the hyperbolic parametric domains with respect to the origin is again demonstrated, as in Fig. 5(a).

By observing Figs. 3–5, it is understood that the most interesting dynamics emerge when the slab is excited by TE waves; therefore, in the following examples the variation of transmissivity will be investigated only for TE polarization. In addition, up to that point, we have considered normal incidence ($\theta = 0^\circ$) and thus the transmitted power does not surpass unity, even though active media are employed. In Fig. 6, we assume an obliquely traveling wave with $\theta = -45^\circ$ and one readily finds that transmission power can be up to four orders of magnitude larger than the incoming one; it is clearly an evidence that the incorporated gain media pump far more energy than that absorbed by the dissipative materials or reflected back at $x \rightarrow -\infty$. In Fig. 6(a), we take $r = 0.4$ and represent $|T_{\text{TE}}|^2$ on the ($\text{Im}[\varepsilon_1]$, $\text{Im}[\varepsilon_2]$) map; the distribution differs from that of Fig. 3(b) as it is asymmetric due to the different filling factors of the two materials. However, the variation across the isolated stable domains in the lower left part of the map can complement well the variation at the unstable domains of the upper right part, like two pieces of a puzzle. This property is related to the interchangeability of the two media and the periodicity of the layered structure of Fig. 1(a). In Fig. 6(b), where $r = 0.5$, the perfect symmetry of Fig. 3(b) is restored since additionally $\text{Re}[\varepsilon_1] = \text{Re}[\varepsilon_2]$. Similar to Fig. 3(b), the response is much stronger at the two islets of stability compared to the upper right region of the considered map; however, as mentioned above, the non-normal incidence substantially enhances the produced power.

C. Configuration plane

Having understood the dynamics of the device when the features of the two employed media (ε_1 , ε_2) are being swept, it is meaningful to show the variation of transmissivity $|T_{\text{TE}}|^2$ with respect to the physical characteristics of the

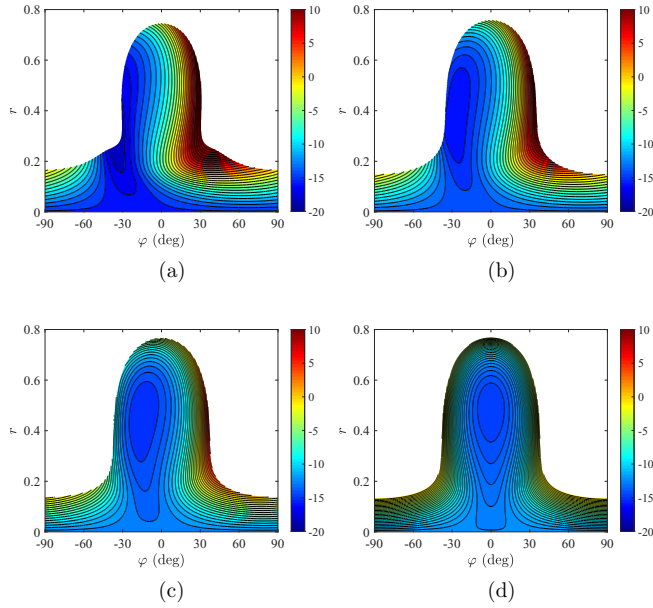


FIG. 7. Transmissivity $|T|^2$ in dB with respect to the optical tilt φ and duty cycle r . (a) $\theta = -45^\circ$, (b) $\theta = -30^\circ$, (c) $\theta = -15^\circ$, and (d) $\theta = 0^\circ$. Plot parameters: $\varepsilon_1 = 1 + i$, $\varepsilon_2 = 1 - 6.5i$, and $h = \lambda/2$. Only TE type of excitation is considered. Blank regions indicate instability.

configuration. In particular, in Fig. 7, we represent the response of the device as a function of the optical tilt φ and duty cycle r for various illumination directions θ . When the tilt angle φ increases, the system is sent to instability for a smaller portion r , since that filling factor corresponds to the active medium. In Fig. 7(a), we assume $\theta = -45^\circ$ and observe a vastly asymmetric response with respect to $\varphi = 0^\circ$, indicating that significant transmissivities are recorded once the sign of φ and θ are opposite ($\varphi\theta < 0$) [34]. More specifically, the device turns to instability for $\varphi > 0$ through huge values, while its output across the symmetric boundary ($\varphi < 0$) is vanishing. An opposite behavior is observed when the incoming angle is taken positive ($\theta > 0$).

In Fig. 7(b), we consider a less obliquely incident wave ($\theta = -30^\circ$) and the obtained transmissivity pattern becomes more symmetric, while the average magnitude of $|T_{TE}|^2$ gets smaller. This trend continues in Figs. 7(c) and 7(d), where the maximal response weakens and the distribution becomes more even with respect to φ . Note that the instability region is only slightly dependent on the incoming direction θ but gets enlarged when the films of the active media are positioned less normally to the boundaries $x = 0, h$. Therefore, the unstable behavior is more probable not only when the corresponding filling factor r increases but also when the optical axis into the anisotropic slab is rotated. It is also remarkable that, regardless of the incidence direction θ , there is a tilt angle φ beyond which the stability of the setup deteriorates substantially since the corresponding boundary in all the four cases of Fig. 7 is almost vertical.

D. Spectra plane

We have considered two types of maps for investigating the operation of the device: one regarding the imaginary (or

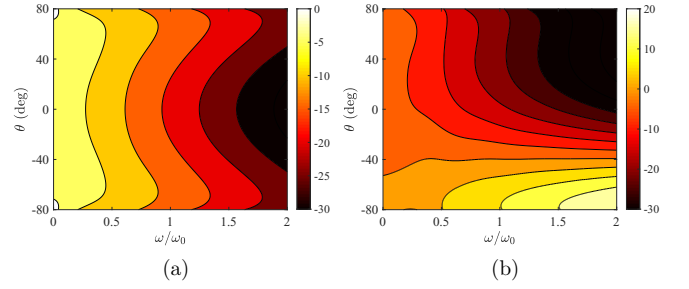


FIG. 8. Transmissivity $|T|^2$ in dB with respect to the relative frequency ω/ω_0 and incoming angle θ . (a) $\varphi = 0^\circ$; (b) $\varphi = 30^\circ$. Plot parameters: $\varepsilon_1 = 1 + i$, $\varepsilon_2 = 1 - 10i$, $r = 0.5$, and $h = \lambda/2$ at $\omega = \omega_0$. Only TE type of excitation is considered. Blank regions indicate instability.

real) parts of the permittivities ($\varepsilon_1, \varepsilon_2$) and one concerning the configuration parameters (φ, r). It would be also stimulating to observe the variation of transmissivity $|T_{TE}|^2$ across the plane of excitation spectra, namely, the oscillation frequency ω (wavelength spectrum) and the direction of incidence θ (angular spectrum). In Fig. 8(a), we consider normally grown flakes ($\varphi = 0^\circ$) and a symmetric distribution of the device response with respect to $\theta = 0^\circ$ is obtained. As indicated by Figs. 3 and 4, when there is no tilt of optical axis or, reciprocally, the incoming wave meets normally the slab boundaries, the output is bounded by unity (even for TE fields). Note that for increasing frequency ω the transmissivity decreases since the slab becomes more opaque and this trend is milder for normal incidence ($\theta = 0^\circ$). Obviously, for $\omega \rightarrow 0$ the setup gets totally transparent ($|T_{TE}| \rightarrow 1$).

In Fig. 8(b), we assume tilted active slabs ($\varphi = 30^\circ$) and, as noted in Fig. 7, a condition $\varphi\theta < 0$ favors transmissivity since the incoming beam is forced to reflect many times between the active flakes and, thus, gradually gains energy at each round trip. In particular, the response is weak and decreasing with frequency when $\varphi\theta > 0$, while being much stronger and an increasing function of ω for $\varphi\theta < 0$. Indeed, for $\varphi\theta > 0$ the losses dominate across the propagation path that belongs almost entirely into the passive host, while for $\varphi\theta < 0$ the incident ray interacts many times with the active medium and, as an avalanche [34], becomes more and more powerful.

IV. CONCLUSIONS

Active multilayers with tilted optical axis formulate a homogenized anisotropic slab that gets obliquely excited by electromagnetic waves. The transfer function of the setup is analytically derived and its poles on the complex frequency plane are obtained; therefore, stability conditions are rigorously deduced under the assumption of dispersion-free media. The transmissivity of the slab is represented across several parametric maps concerning the employed gain or lossy materials, the geometry specifications, and the excitation spectra; in this way, one can tune the system to transmit power several orders of magnitude larger than the incoming one, without taking the risk of instability.

An interesting expansion of the presented study would be to optimize the structure and the texture of the specific layout so that various types of responses are maximized, once paired to the suitable excitation. In this sense, the existence or nonexistence of the limits in the performance of this class of active designs will be reported while respecting the stability conditions. The recorded supreme efficiencies would help to express the corresponding scores of passive designs as a fraction of them and serve the role of bars for more complicated structures employing more sophisticated gain media to pass.

ACKNOWLEDGMENTS

The author would like to thank Prof. A. Sihvola (Aalto University, Espoo, Finland) and Prof. F. Monticone (Cornell University, Ithaca, NY, USA) for enlightening discussions on the effective-medium theory breakdown and the emergence of unstable poles in the transfer functions of active photonic systems, respectively. This work was partially supported by Nazarbayev University Faculty Development Competitive Research Grant No. 021220FD4051 (“*Optimal design of photonic and quantum metamaterials*”).

-
- [1] A. D. Boardman, V. V. Grimalsky, Y. S. Kivshar, S. V. Koshevaya, M. Lapine, N. M. Litchinitser, V. N. Malnev, M. Noginov, Y. G. Rapoport, and V. M. Shalaev, Active and tunable metamaterials, *Laser Photon. Rev.* **5**, 287 (2011).
- [2] H.-T. Chen, W. J. Padilla, J. M. O. Zide, A. C. Gossard, A. J. Taylor, and R. D. Averitt, Active terahertz metamaterial devices, *Nature (London)* **444**, 597 (2006).
- [3] M. Selvanayagam and G. V. Eleftheriades, Experimental Demonstration of Active Electromagnetic Cloaking, *Phys. Rev. X* **3**, 041011 (2013).
- [4] J. Rensberg, S. Zhang, Y. Zhou, A. S. McLeod, C. Schwarz, M. Goldflam, M. Liu, J. Kerbusch, R. Nawrodt, S. Ramanathan, D. N. Basov, F. Capasso, C. Ronning, and M. A. Kats, Active optical metasurfaces based on defect-engineered phase-transition materials, *Nano Lett.* **16**, 1050 (2016).
- [5] B. O. Zhu, J. Zhao, and Y. Feng, Active impedance metasurface with full 360° reflection phase tuning, *Sci. Rep.* **3**, 3059 (2013).
- [6] W. Zhou, M. Dridi, J. Y. Suh, C. H. Kim, D. T. Co, M. R. Wasielewski, G. C. Schatz, and T. W. Odom, Lasing action in strongly coupled plasmonic nanocavity arrays, *Nat. Nanotechnol.* **8**, 506 (2013).
- [7] L. Feng, Z. J. Wong, R.-M. Ma, Y. Wang, and X. Zhang, Single-mode laser by parity-time symmetry breaking, *Science* **346**, 6212 (2014).
- [8] M. A. Noginov, G. Zhu, A. M. Belgrave, R. Bakker, V. M. Shalaev, E. E. Narimanov, S. Stout, E. Herz, T. Suteewong, and U. Wiesner, Demonstration of a spaser-based nanolaser, *Nature (London)* **460**, 1110 (2009).
- [9] A. Regensburger, C. Bersch, M.-A. Miri, G. Onishchukov, D. N. Christodoulides, and U. Peschel, Parity-time synthetic photonic lattices, *Nature (London)* **488**, 167 (2012).
- [10] L. Feng, Y.-L. Xu, W. S. Fegadolli, M.-H. Lu, J. E. B. Oliveira, V. R. Almeida, Y.-F. Chen, and A. Scherer, Experimental demonstration of a unidirectional reflectionless parity-time metamaterial at optical frequencies, *Nat. Mater.* **12**, 108 (2013).
- [11] N. V. Alexeeva, I. V. Barashenkov, A. A. Sukhorukov, and Y. S. Kivshar, Optical solitons in PT-symmetric nonlinear couplers with gain and loss, *Phys. Rev. A* **85**, 063837 (2012).
- [12] Multidisciplinary University Research Initiative (MURI) Awards, Active and Reconfigurable Topological Mechanical Metamaterials from the Nanoscale to the Macroscale, PI: X. Mao, University of Michigan, 2020, <https://www.cto.mil/2020-muri/>.
- [13] National Science Foundation (NSF) Awards, Advanced Functional Metamaterials, PI: M. Noginov, Norfolk State University, 2017, https://www.nsf.gov/awardsearch/showAward?AWD_ID=1205457.
- [14] National Science Foundation (NSF) Awards, Center for Hybrid, Active, and Responsive Materials, PI: T. Epps, University of Delaware, 2020, https://nsf.gov/awardsearch/showAward?AWD_ID=2011824&HistoricalAwards=false.
- [15] A. Krasnok, D. Baranov, H. Li, M.-A. Miri, F. Monticone, and A. Alù, Anomalies in light scattering, *Adv. Opt. Photon.* **11**, 892 (2019).
- [16] P. Lalanne, W. Yan, K. Vynck, C. Sauvan, and J.-P. Hugonin, Light interaction with photonic and plasmonic resonances, *Laser Photon. Rev.* **12**, 1700113 (2018).
- [17] M. Piccardo, B. Schwarz, D. Kazakov, M. Beiser, N. Opačak, Y. Wang, S. Jha, J. Hillbrand, M. Tamagnone, W. T. Chen, A. Y. Zhu, L. L. Columbo, A. Belyanin, and F. Capasso, Frequency combs induced by phase turbulence, *Nature (London)* **582**, 360 (2020).
- [18] V. Kovanis, A. Gavrielides, T. B. Simpson, and J. M. Liu, Instabilities and chaos in optically injected semiconductor lasers, *Appl. Phys. Lett.* **67**, 2780 (1995).
- [19] Y. Zhiyenbayev, Y. Kominis, C. Valagiannopoulos, V. Kovanis, and A. Bountis, Enhanced stability, bistability, and exceptional points in saturable active photonic couplers, *Phys. Rev. A* **100**, 043834 (2019).
- [20] S. A. H. Gangaraj, B. Jin, C. Argyropoulos, and F. Monticone, Broadband Field Enhancement and Giant Nonlinear Effects in Terminated Unidirectional Plasmonic Waveguides, *Phys. Rev. Appl.* **14**, 054061 (2020).
- [21] C. Valagiannopoulos and V. Kovanis, Injection-locked photonic oscillators: Legacy results and future applications, *IEEE Antennas Propag. Mag.* **63**, 51 (2021).
- [22] A. Chen and F. Monticone, Active scattering-cancellation cloaking: Broadband invisibility and stability constraints, *IEEE Trans. Antennas Propag.* **68**, 1655 (2020).
- [23] D. L. Sounas, R. Fleury, and A. Alù, Unidirectional Cloaking Based on Metasurfaces with Balanced Loss and Gain, *Phys. Rev. Appl.* **4**, 014005 (2015).
- [24] M. Moccia, G. Castaldi, A. Alù, and V. Galdi, Harnessing spectral singularities in non-Hermitian cylindrical structures, *IEEE Trans. Antennas Propag.* **68**, 1704 (2020).
- [25] B. Yezhezep and C. Valagiannopoulos, Approximate stability dynamics of concentric cylindrical metasurfaces, *IEEE Trans. Antennas Propag.* **68**, 5716 (2021).
- [26] F. Monticone, C. A. Valagiannopoulos, and A. Alù, Parity-Time Symmetric Nonlocal Metasurfaces: All-Angle Negative

- Refraction and Volumetric Imaging, *Phys. Rev. X* **6**, 041018 (2016).
- [27] S. Savoia, C. A. Valagiannopoulos, F. Monticone, G. Castaldi, V. Galdi, and A. Alù, Magnified imaging based on non-Hermitian nonlocal cylindrical metasurfaces, *Phys. Rev. B* **95**, 115114 (2017).
- [28] E. Ugarte-Muñoz, S. Hrabar, D. Segovia-Vargas, and A. Kirichenko, Stability of non-Foster reactive elements for use in active metamaterials and antennas, *IEEE Trans. Antennas Propag.* **60**, 3490 (2012).
- [29] A. C. Tasolamprou, L. Zhang, M. Kafesaki, T. Koschny, and C. M. Soukoulis, Experimentally excellent beaming in a two-layer dielectric structure, *Opt. Express* **22**, 23147 (2014).
- [30] J. Lončar, S. Hrabar, and D. Muha, Stability of simple lumped-distributed networks with negative capacitors, *IEEE Trans. Antennas Propag.* **65**, 390 (2017).
- [31] J. Valentine, S. Zhang, T. Zentgraf, E. Ulin-Avila, D. A. Genov, G. Bartal, and X. Zhang, Three-dimensional optical metamaterial with a negative refractive index, *Nature (London)* **455**, 376 (2008).
- [32] B. Wood, J. B. Pendry, and D. P. Tsai, Directed subwavelength imaging using a layered metal-dielectric system, *Phys. Rev. B* **74**, 115116 (2006).
- [33] A. Poddubny, I. Iorsh, P. Belov, and Y. Kivshar, Hyperbolic metamaterials, *Nat. Photon.* **7**, 948 (2013).
- [34] T. Zhumabek and C. Valagiannopoulos, Light trapping by arbitrarily thin cavities, *Phys. Rev. Res.* **2**, 043349 (2020).
- [35] S. Liu, H. Chen, and T. J. Cui, A broadband terahertz absorber using multilayer stacked bars, *Appl. Phys. Lett.* **106**, 151601 (2015).
- [36] F. Ding, Y. Cui, X. Ge, Y. Jin, and S. He, Ultra-broadband microwave metamaterial absorber, *Appl. Phys. Lett.* **100**, 103506 (2012).
- [37] B. Wang, X. Zhang, F. J. Garcia-Vidal, X. Yuan, and J. Teng, Strong Coupling of Surface Plasmon Polaritons in Monolayer Graphene Sheet Arrays, *Phys. Rev. Lett.* **109**, 073901 (2012).
- [38] H. Yan, X. Li, B. Chandra, G. Tulevski, Y. Wu, M. Freitag, W. Zhu, P. Avouris, and F. Xia, Tunable infrared plasmonic devices using graphene/insulator stacks, *Nat. Nanotechnol.* **7**, 330 (2012).
- [39] R. Maas, J. Parsons, N. Engheta, and A. Polman, Experimental realization of an epsilon-near-zero metamaterial at visible wavelengths, *Nat. Photon.* **7**, 907 (2013).
- [40] P. Moitra, Y. Yang, Z. Anderson, I. I. Kravchenko, D. P. Briggs, and J. Valentine, Realization of an all-dielectric zero-index optical metamaterial, *Nat. Photon.* **7**, 791 (2013).
- [41] D. Tulegenov and C. Valagiannopoulos, Uniaxial films of maximally controllable response under visible light, *Sci. Rep.* **10**, 13051 (2020).
- [42] J. Yoon, S. Jo, I. S. Chun, I. Jung, H.-S. Kim, M. Meitl, E. Menard, X. Li, J. J. Coleman, U. Paik, and J. A. Rogers, GaAs photovoltaics and optoelectronics using releasable multilayer epitaxial assemblies, *Nature (London)* **329**, 465 (2010).
- [43] H. H. Sheinfux, I. Kaminer, Y. Plotnik, G. Bartal, and M. Segev, Subwavelength Multilayer Dielectrics: Ultrasensitive Transmission and Breakdown of Effective-Medium Theory, *Phys. Rev. Lett.* **113**, 243901 (2014).
- [44] T. T. Koutserimpas and R. Fleury, Electromagnetic waves in a time periodic medium with step-varying refractive index, *IEEE Trans. Antennas Propag.* **66**, 5300 (2018).
- [45] A. H. Sihvola, *Electromagnetic Mixing Formulas and Applications*, IEE Electromagnetic Waves Series: Institution of Electrical Engineers (IEEE, New York, 1999).
- [46] S. V. Zhukovsky, A. Andryieuski, O. Takayama, E. Shkondin, R. Malureanu, F. Jensen, and A. V. Lavrinenko, Experimental Demonstration of Effective Medium Approximation Breakdown in Deeply Subwavelength All-Dielectric Multilayers, *Phys. Rev. Lett.* **115**, 177402 (2015).
- [47] H. H. Sheinfux, I. Kaminer, A. Z. Genack, and M. Segev, Interplay between evanescence and disorder in deep subwavelength photonic structures, *Nat. Commun.* **7**, 12927 (2016).
- [48] H. H. Sheinfux, Y. Lumer, G. Ankonina, A. Z. Genack, G. Bartal, and M. Segev, Observation of Anderson localization in disordered nanophotonic structures, *Science* **356**, 953 (2017).
- [49] M. A. Kats, R. Blanchard, P. Genevet, and F. Capasso, Nanometre optical coatings based on strong interference effects in highly absorbing media, *Nat. Mater.* **12**, 20 (2012).
- [50] COMSOL Multiphysics® v. 5.6, www.comsol.com, COMSOL AB, Stockholm, Sweden.
- [51] C. Valagiannopoulos and S. A. Tretyakov, Stability of active photonic metasurface pairs, *New J. Phys.* **23**, 113045 (2021).
- [52] K. G. Makris, Z. H. Musslimani, D. N. Christodoulides, and S. Rotter, Constant-intensity waves and their modulation instability in non-Hermitian potentials, *Nat. Commun.* **6**, 7257 (2015).
- [53] A. Brandstötter, K. G. Makris, and S. Rotter, Scattering-free pulse propagation through invisible non-Hermitian disorder, *Phys. Rev. B* **99**, 115402 (2019).
- [54] S. Yu, X. Piao, and N. Park, Bohmian Photonics for Independent Control of the Phase and Amplitude of Waves, *Phys. Rev. Lett.* **120**, 193902 (2018).
- [55] H. M. Nussenzveig, *Causality and Dispersion Relations* (Academic Press, New York, 1972).
- [56] Z. Hayran, A. Chen, and F. Monticone, Spectral causality and the scattering of waves, *Optica* **8**, 1040 (2021).